DOT/FAA/21/07
Office of Aerospace Medicine
Washington, DC 20591

Federal Aviation Administration

Simulation of Oblique Loading Configurations Using an FAA Hybrid III Virtual Anthropomorphic Test Device

David M. Moorcroft

Civil Aerospace Medical Institute
Federal Aviation Administration
Oklahoma City, OK 73125

March 2021

NOTICE

This publication and all Office of Aerospace Medicine technical reports are available in full-text from the
Civil Aerospace Medical Institute's publications website: http://www.faa.gov/go/oamtechreports

Technical Report Documentation Page

1. Report No.	2. Government Accession No.	3. Recipient's Catalog No.
DOT/FAA/21/07		

4. Title and Subtitle	5. Report Date
Simulation of Oblique Loading Configurations Using an FAA Hybrid III virtual Anthropomorphic Test Device	March 2021
	6. Performing Organization Code

7. Author(s)	8. Performing Organization Report No.
Moorcroft, David M.	

9. Performing Organization Name and Address	10. Work Unit No. (TRAIS)
FAA Civil Aerospace Medical Institute P.O. Box 25082 Oklahoma City, OK 73125	11. Contract or Grant No.

12. Sponsoring Agency Name and Address	13. Type of Report and Period Covered
Office of Aerospace Medicine Federal Aviation Administration 800 Independence Ave., S.W. Washington, DC 20591	14. Sponsoring Agency Code

15. Supplemental Notes

Project No. 2013-AAM-632-DYN-10079.

16. Abstract

Anthropomorphic test device (ATD) construction and instrumentation is optimized for the loading direction the ATD is intended to evaluate. The optimization of these ATDs limits the ability of the ATD to predict occupant injury in an impact direction that significantly deviates from the design basis. With the introduction of herring bone configurations in transport category aircraft, there is a need to evaluate oblique angles, however, no ATD has been designed to evaluate these angles specifically. This report details simulations exploring occupant kinematics of the Federal Aviation Administration (FAA)Hybrid III in oblique loading configurations. The Madymo multi-body FAA Hybrid III model was placed in a rigid seat, with and without an armrest, and restrained with and without a shoulder belt. The lap belt was a combination of body-centered and traditional lap belts. Simulations were run with loading vectors of 0°, 30°, 45°, and 60° at two pulse levels for a total of 32 runs. Data from similar tests in eight configurations were used to establish a baseline level of correlation for the virtual ATD (v-ATD). The simulations were then used to look for trends in the configurations.

The model performed marginally in the configurations simulated for this project. The different distribution of loads between the lumbar and T12 locations suggests that the interaction of the lap belt on the pelvis may be inaccurate, something that was previously observed in early versions of the Madymo Hybrid II (since corrected). The trend analysis for the lap belt only configurations suggests that spinal Fz load decreases with impact angle, which, if reproducible, would assist in defining a critical installation angle for certification testing for the current injury criteria. The Madymo FAA Hybrid III v-ATD appears to require further evaluation, and possible changes, before it can be used to accurately predict occupant injury in oblique loading configurations.

17. Key Words	18. Distribution Statement
Oblique Loading, Virtual ATD, v-ATD, Dynamic Test, Lumbar Tension	

19. Security Classif. (of this report)	20. Security Classif. (of this page)	21. No. of Pages	22. Price
Unclassified	Unclassified	33	

ACKNOWLEDGMENTS

Research reported in this paper was conducted under the sponsorship of the FAA Office of Aerospace Medicine and was accomplished by the Aerospace Medical Research Division, Protection and Survival Research Branch, Engineering Sciences Section, Biodynamics Research Team (AAM-632), at the FAA Civil Aerospace Medical Institute. This work was performed under project No. 2013-AAM-632-DYN-10079.

The tests referenced herein would not have been completed without the support of the technical staff at CAMI: Richard DeWeese, Amanda Taylor, David DeSelms, Ronnie Minnick, Jeffrey Ashmore, and Jim Biegler (contractor). Ian Hellstrom provided assistance with the formatting of the document. Restraints were provided by AmSafe Corp. Commercial Aviation.

DISCLAIMER

Reference to any product or service should not be construed as an endorsement.

Contents

List of Figures

List of Tables

Simulation of Oblique Loading Configurations Using an FAA Hybrid III Virtual Anthropomorphic Test Device

BACKGROUND

Anthropomorphic test device (ATD) construction and instrumentation is optimized for the loading direction that the ATD is intended to evaluate. The optimization of these ATDs limits the ability of the ATD to predict occupant injury in an impact direction that significantly deviates from the design basis. Transport category passenger seats continue to evolve, with the latest development being a partially enclosed (pod) seat that is oriented obliquely with respect to the aircraft centerline in what is commonly referred to as a "herringbone" arrangement. This orientation exceeds the standard 18° of a forward-facing seat but is not purely side facing. No ATD has been designed to specifically evaluate the range of angles that comprise oblique seats or the effect of the greater occupant flail that can occur in aviation seat configurations compared to automotive configurations.

Current Federal Aviation Administration (FAA) regulations and policies call out two ATDs designed explicitly for forward impacts, the Hybrid II and FAA Hybrid III, as well as one ATD designed for lateral impacts, the ES-2re [1-3]. The ES-2re is constructed such that it cannot bend properly when the loading allows for forward flail and would likely incur significant damage. Therefore this ATD is not suitable for evaluating oblique loading. The Hybrid II is constructed such that it can withstand oblique loading without damage, but it offers a limited array of sensors. The FAA Hybrid III has a similar construction to the Hybrid II, sharing some parts, and offers a wider array of instrumentation, making it the logical choice to support an evaluation of oblique loading in aviation seats. In the time between the initiation of this research and the publication of the report, the FAA released a policy statement in which the FAA Hybrid III ATD is specified for certification testing of oblique seats [4]. The policy requires that lumbar spine tension (Fz) not exceed 1200 lb.

Oblique Seat Testing

The FAA Biodynamics Research Team at the Civil Aerospace Medical Institute (CAMI) is in the middle of a multi-year project to determine injury criteria for obliquely oriented seats. The project includes an evaluation of the unique occupant kinematics and loading that can occur in impacts involving oblique seat installations, identifying loading conditions that cannot be adequately assessed using existing forward or lateral injury criteria. The project also includes a determination of the injury mechanisms, the human impact tolerance levels, and methods of predicting occupant injuries in obliquely facing seats during a survivable crash. As part of this project, CAMI conducted a series of oblique seat tests with a rigid seat and the 14 CFR 25.562 longitudinal crash pulse [1]. This includes lap belt-only testing conducted in 2012 [5] and tests with a shoulder harness, as shown in Figure 1, conducted in 2016 [full publication forthcoming]. The lap belt only tests were run to assess the occupant kinematics and loading

conditions present in the earliest oblique seat designs. The tests with a shoulder harness were run to quantify the effect of limiting torso flail on the spinal loads.

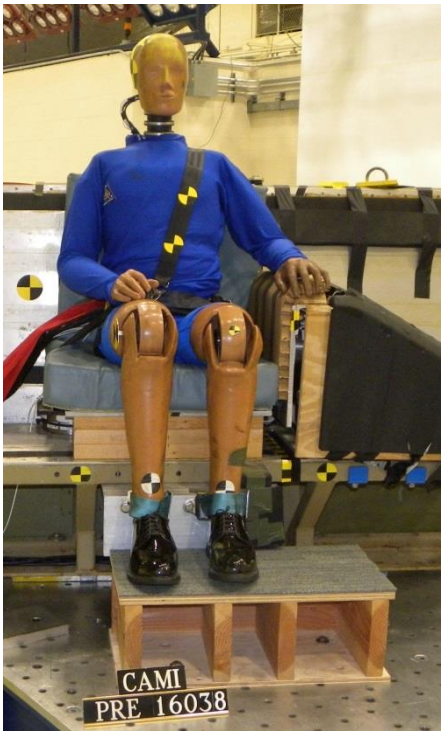

Figure 1: Oblique Seat Test with Armrest and Shoulder Harness

To determine the types of injuries that can occur and to define appropriate injury criteria, the FAA is working with the Medical College of Wisconsin (MCW). MCW has conducted postmortem human subject and ATD tests in order to develop a preliminary injury criterion for lumbar spine tension injuries [6-8]. These tests used the same seat configuration as the CAMI tests (lap belt only tests) and multiple impact pulses that were scaled off the standard 16g pulse.

ATD Simulations

Just as the physical FAA Hybrid III development focused on horizontal and vertical test performance, the FAA Hybrid III virtual ATDs (v-ATDs) were developed based on performance in those impact directions. To the author's knowledge, no previous research has been conducted to evaluate the performance of the FAA Hybrid III v-ATD in this loading scenario. This report details simulations exploring occupant kinematics of the Madymo FAA Hybrid III v-ATD (TASS International, Helmond, The Netherlands) in oblique loading configurations. There are two purposes for this work. First, as the aviation seating industry increases the number of oblique seats and increases their use of computer models within certification, it is essential to understand how the v-ATD performs in this unique loading environment. Second, simulations are ideal for trend analysis as there is no variability between simulation setup conditions (i.e., test-to-test variability is absent). To the second purpose, this project explores the effect of belt configuration and impact angle on occupant kinematics. The

primary output of this work is to determine if the evaluated v-ATD is appropriate for use in these scenarios.

MODEL CONSTRUCTION

A single model was used as a baseline for all simulations. This model consisted of multi-body rigid planes that represented the CAMI rigid seat. The Madymo FAA Hybrid III v-ATD was lowered into the seat with gravity acting in the vertical direction and one-quarter gravity acting in the negative X-direction. One-quarter gravity applied approximately 20 lb to the chest of the v-ATD. Once the v-ATD was settled, the arms and legs were manually placed in position. This seating method is consistent with the procedure defined in SAE International Aerospace Standard 8049C [9].

Rigid Seat

The baseline model consisted of four planes: a floor, seat pan, seat bottom cushion, and seat back cushion. The seat pan plane was for visual reference only; no contact parameters were defined. For the armrest configuration, a nearly rectangular cylinder (degree parameter of 50) was defined to match the height and width of the physical armrest (Figure 2). A cylinder was selected to avoid potential edge effects that might occur if planes were used. The cylinder is a simplification of the actual geometry, focused on the two surfaces that the ATD contacts. The left-arm placement was modified so the arm laid atop the armrest, as was done in the corresponding physical tests. Figure 2 shows the v-ATD arm placement with and without the armrest, while Figure 1 shows the test placement.

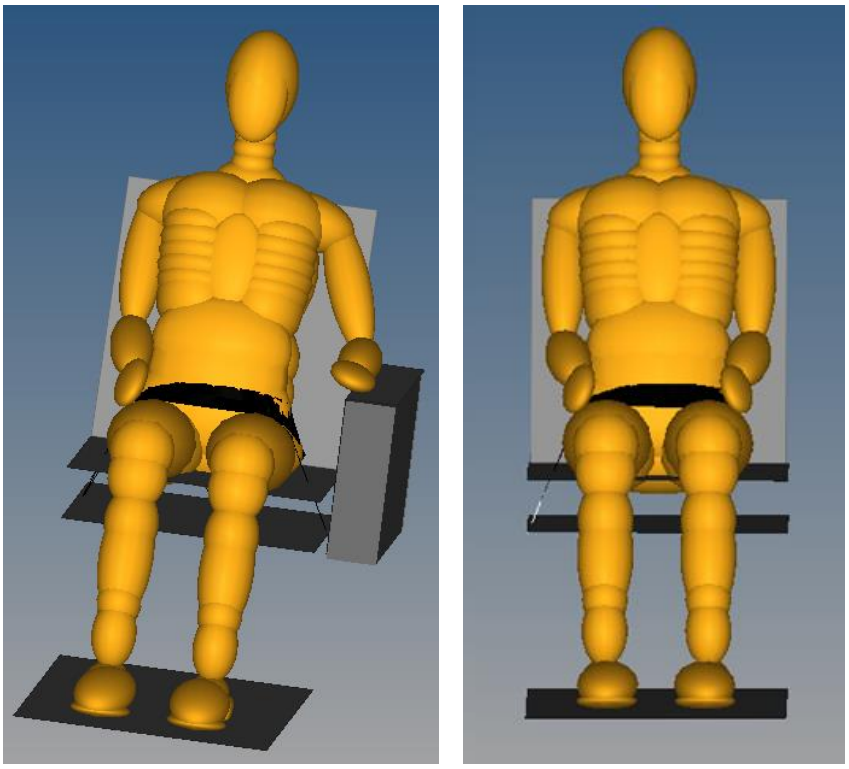

Figure 2: Model of Seat with Armrest (L) and without Armrest (R)

The seat dimensions match the configuration tested at CAMI, as shown in Figures 3 and 4 [8]. The seat pan is flat and oriented 0° with respect to horizontal, while the seat back is reclined 13° with respect to vertical. The armrest, lined with 1-inch cardboard honeycomb, abuts the edge of the seat pan and extends up 12.4 inches above the seat pan. Load cells were placed at the three lap belt anchor locations and attached to the armrest. The seat includes a 4-inch thick, soft open cell foam cushion with a leather cover. The floor was lined with carpet. In Figures 3 and 4, the plus signs denote the lap belt anchor positions. Not shown is the shoulder belt guide, whose centerline was 3.3 inches forward of the seat centerline.

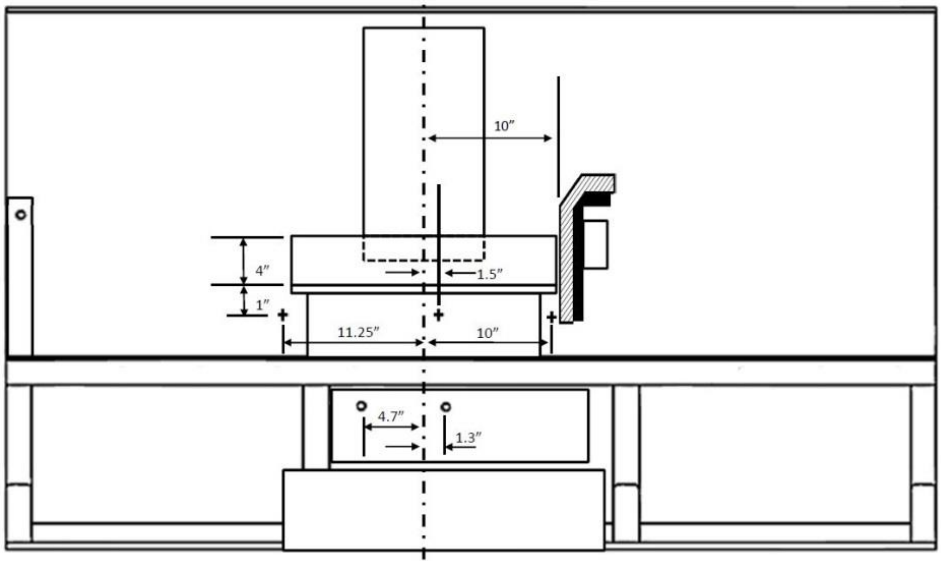

Figure 3: Rigid Seat Dimensions (Front View)

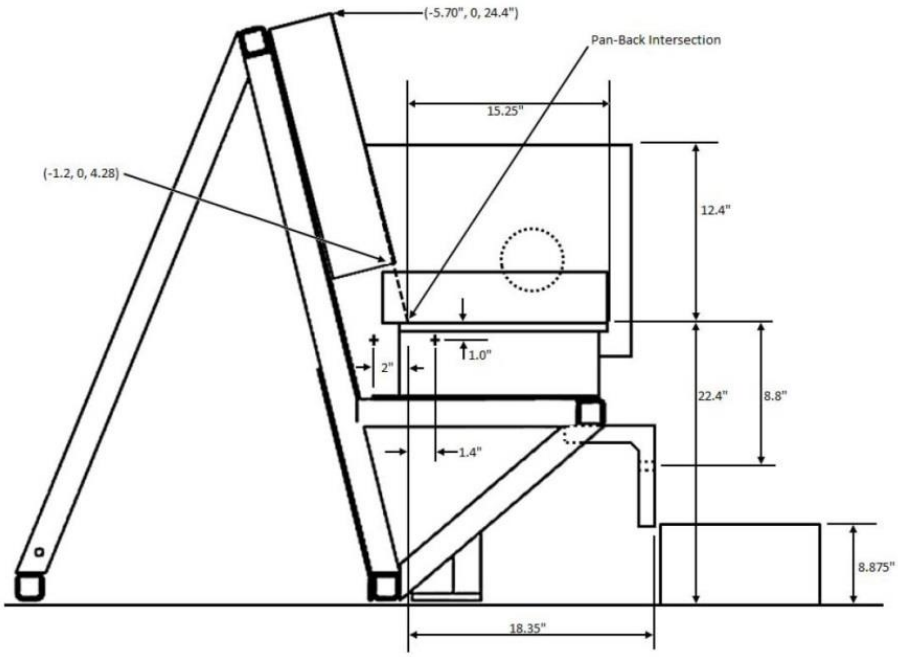

S

Figure 4: Rigid Seat Dimensions (Side View)

v-ATD

Simulations were run with the Madymo virtual representation of the FAA Hybrid III, version 1.8. This model is a composite of the Madymo Hybrid II and Hybrid III multi-body models. The model is a series of ellipsoid surfaces attached to rigid bodies that are connected by numerical joints. The v-ATD was evaluated by the developer using a simulation of the pendulum impactor test specified for physical ATD chest compression calibration [10]. The physical thorax is a combination of two ATDs and their respective chest compression corridors do not overlap. The source of the data used by the v-ATD developer is not known and no standard has been defined by the FAA. It does not appear that the v-ATD developer compared the model performance to the other component tests for the ATD, as defined in 49 CFR 572 [11]. The v-ATD was also compared against dynamic tests for pure frontal, pure vertical, and combined horizontal/vertical (60°) configurations [10]. All defined v-ATD models in Madymo use the international system of units (SI units) and require that the rest of the model is also defined in SI units. As is expected in aviation, US customary units are used throughout this report. Inputs into the model were converted to SI units and model outputs were converted back to US customary units following standard rounding practice.

The baseline FAA Hybrid III model includes all outputs that are typically included in physical testing, including upper and lower neck loads, lumbar load, and the T12 load. Angular rate sensors were added to this model and placed at the head center of gravity (CG) (CG of the head body), chest (CG of the thoracic spine body), and pelvis (CG of the pelvis body). The position of the head CG and H-point were also included in the outputs. The Head Injury Criteria (HIC) was not evaluated as head contact with support structures was not expected in these scenarios.

Restraints

Two restraint configurations were included, 1) a combination of a body centered lap belt and a conventional lap belt, and 2) a body-centered lap belt with shoulder harness combined with the conventional lap belt. For the conventional lap belt, a sample finite element (FE) lap belt was selected from the Madymo application library and fitted around the settled v-ATD using the belt fitting tool in XMADgic (version 7.6.1, TASS International, Helmond, The Netherlands). This belt includes Madymo belt segments at the ends, which are effectively 1D tension-only spring elements. The combination of FE and spring elements is referred to as a hybrid belt [12]. This fitment was retained for all simulations.

For the body-centered lap belt with no shoulder harness, a 30-inch-long rectangular surface was created and meshed using triangular 2D membrane elements in HyperMesh (Version 14.0, Altair, Troy, MI). The mesh was imported into Madymo and manually fitted around the v-ATD by pulling on truss elements temporarily attached to both ends of the FE belt (Figure 5). During the fitting, the truss element properties were defined such that they elongated at a tension of approximately 10 lb, which is in the range of recommended values to achieve the required "two finger tight" [12]. To get proper fit, the side of the belt that connects to the center belt attachment location was pulled earlier than the other side. Once completed, the truss elements were replaced by Madymo belt segments (Figure 6).

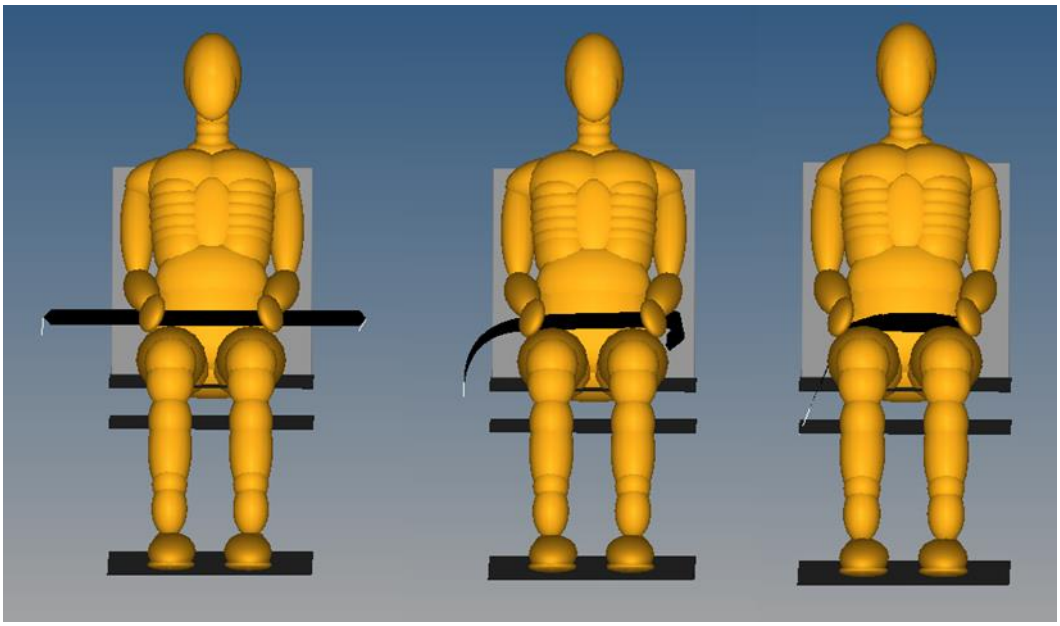

Figure 5: Manual Belt Fitting T = 0ms (L), T = 125ms (C), T = 200ms (R)

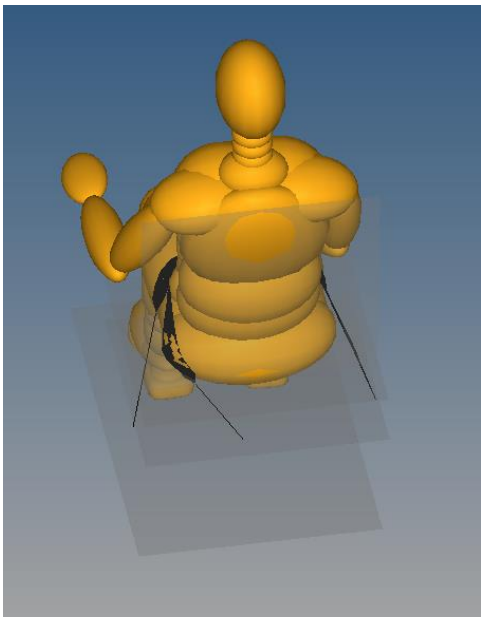

Figure 6: Body-Centered Belt Wrapped Around Pelvis (Left Arm Raised)

For the body-centered belt with a shoulder harness, a separate three-point belt was used. This belt was previously used in side-facing simulations with an ES-2re v-ATD [13]. This belt consists of three FE segments (left lap belt, right lap belt, and shoulder belt) which are supported on a buckle ellipsoid via three truss elements (Figure 7). The manual fitting procedure mentioned above was used to fit this belt, including moving the center attachment end first, followed by the other lap belt section, and finally the shoulder belt. This is the same tightening order used in the physical setup. Once fit, the FE belts were connected to the seat attachment points with the 1D Madymo belt segments (Figure 8). In the physical tests, the buckle that attached the shoulder belt to the lap belt ranged from the seat centerline to 1.0 inches behind the seat centerline. In the model, the buckle was approximately 1.85 inches behind the seat centerline.

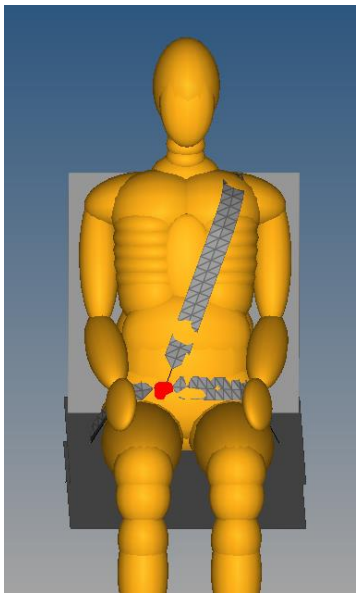

Figure 7: Belt with Shoulder Harness (Buckle Ellipsoid Shown in Red)

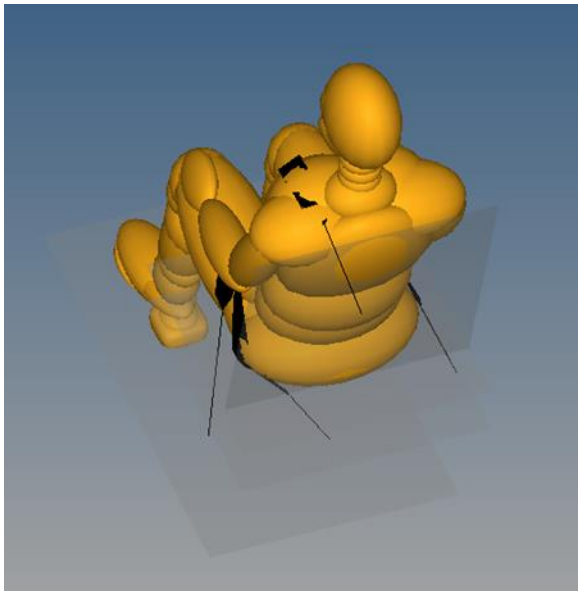

Figure 8: Rear View showing Body-Centered Belt Fit

Shoulder Strap Payout

The shoulder harness used in the physical tests included a retractor with an inertia reel. When the belt is suddenly pulled, such as during the impact event, the reel locks causing the retractor to act as a rigid anchor point. Due to the retractor's properties, some webbing pays out of the retractor during the dynamic event. The total payout was measured during the tests using a simplified string pot. The specific properties of the inertia reel were not available for the model, so the properties were assumed based on the test data. Shoulder belt payout was available for five tests, with an average payout of 1.2 inches (range, 1.0 inch to 1.4 inch). The peak shoulder belt load averaged 1388 lb (range, 1360 lb to 1405 lb). A linear force-payout function using the averages from the physical tests was used in the model. The numerical

retractor was initially free to payout. Five milliseconds into the event the reel was locked and any further payout is based on the defined force-payout function.

Belt Properties

All FE segments were 1.9 inches wide with a thickness of 0.0475 inches and a density of 0.035588 lb/in^3. These values are based on the physical polyester belts and the material data sheet provided with webbing. The values also fit within the range of values defined in Aerospace Recommended Practice 5765 [12]. The material model selected was the HYSISO (isotropic material model with hysteresis) with stress-strain properties based on belt testing completed in-house (Figure 9). A linear strain formulation was used. These properties were scaled to provide equivalent force-deflection characteristics for the 1D segments. At the ends of the FE belts, two elements were defined as rigid to replicate the metal ends and provide a stable support for the 1D belt segments (Figure 10).

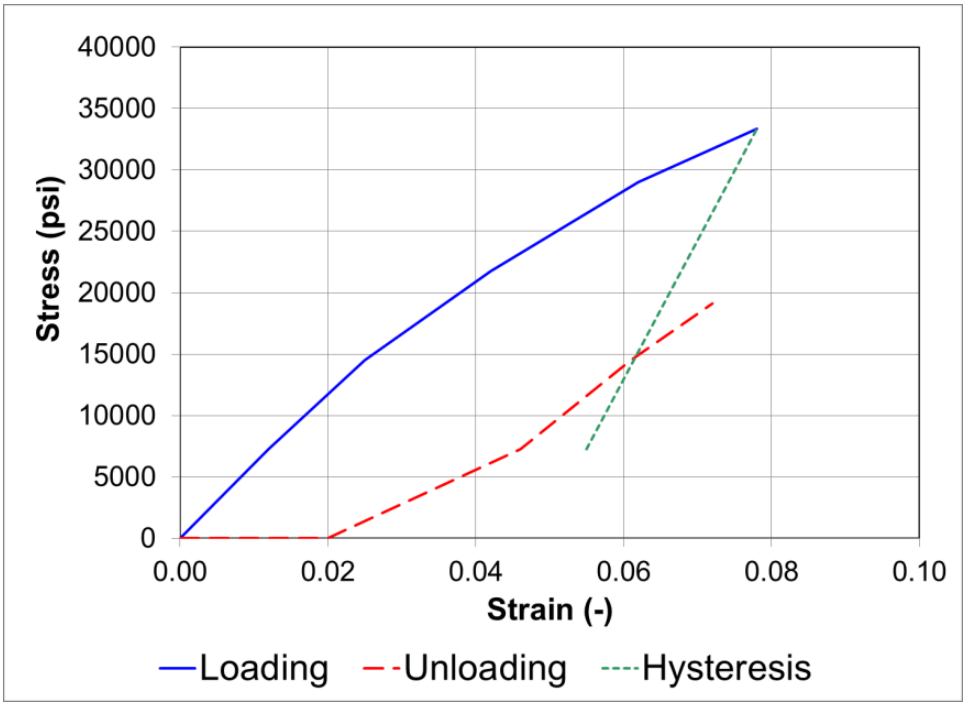

Figure 9: Plot of Finite Element Belt Properties

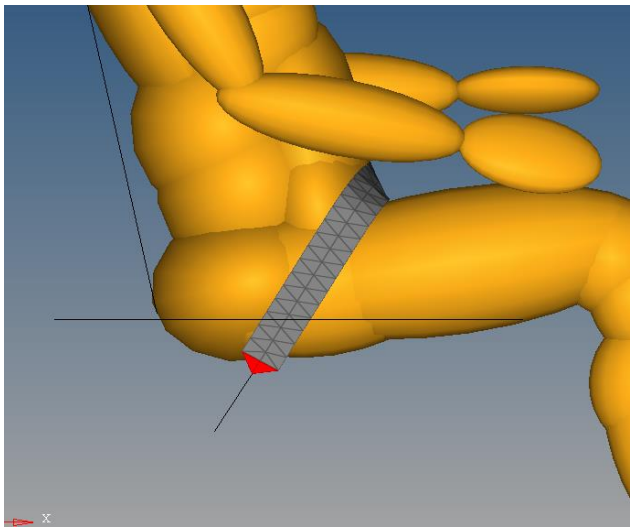

Figure 10: Lap Belt with Rigid Elements Shown in Red

Contact

Force-penetration based contacts were defined between the v-ATD and seat planes. For the seat bottom cushion, only the properties of the seat cushion were used (i.e. the deformation of the ATD pelvis was ignored). The force-penetration characteristics of the seat bottom cushion were based on in-house testing of the foam (Figure 11). For the seatback, floor, and armrest (when included), only the characteristics of the v-ATD were used. This effectively assumes that the seat components are rigid. For the seatback, this represents the 2012 tests [5] which included a stiff closed cell foam for positioning purposes, not the 2016 tests with a soft open cell foam seatback cushion [full publication forthcoming].

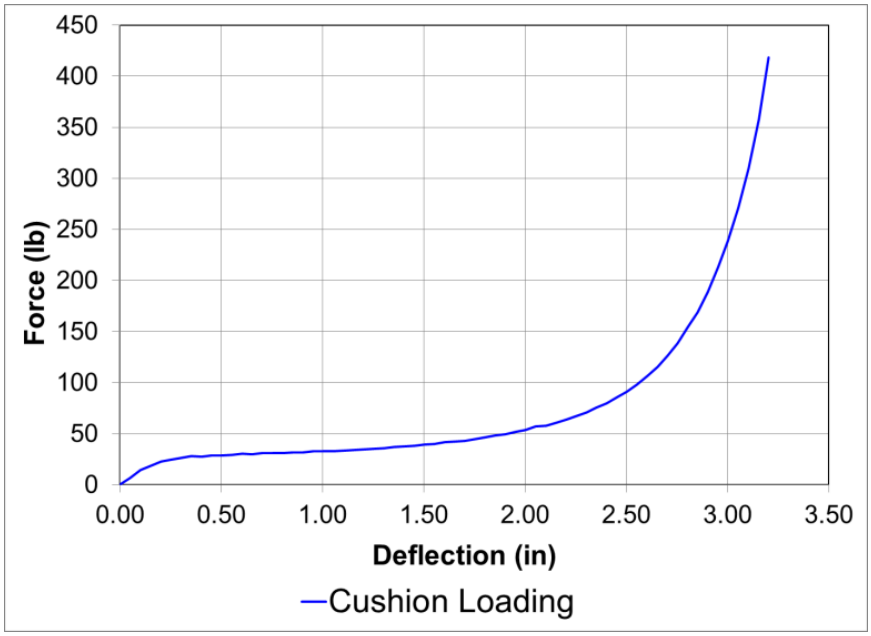

Figure 11: Plot of Foam Properties

Contact between the FE belts and the v-ATD were also defined as force-penetration, using the properties of the v-ATD. Note that in the case of an FE belt, the belt elongation characteristics still affect the interaction. No contact was defined between the belts and the seat planes or between the 1D belt segments and the v-ATD. No contact was defined between the body centered lap belt and the conventional lap belt (to avoid numerical instabilities).

Model Outputs

In addition to the v-ATD outputs, the force in the 1D-belt segments and the force acting on the armrest (when included) was calculated. As such, all signals measured in the physical CAMI tests were also available in the simulation results. A quantitative kinematic analysis of the test data is currently unavailable. As a result, this report will focus on the primary measured loads (i.e., spinal tension in the z-direction, belt forces, and armrest contact force).

Sled Pulse and Seat Installation Angles

In a typical crash, the vehicle is decelerated. The most pertinent interaction is the relative motion of the occupant to the vehicle. For the purposes of modeling a sled test, it is simplest to apply a uniform acceleration field to the occupant while keeping the seat fixed. Two sled pulses were defined for this project: 16g and 9.6g. The lower pulse corresponds to the 60% pulse tested at MCW, which is an isosceles triangle with a peak G that is 60% of the 16g pulse (Figure 12). All pulses initiated at time zero and stopped at 180 ms.

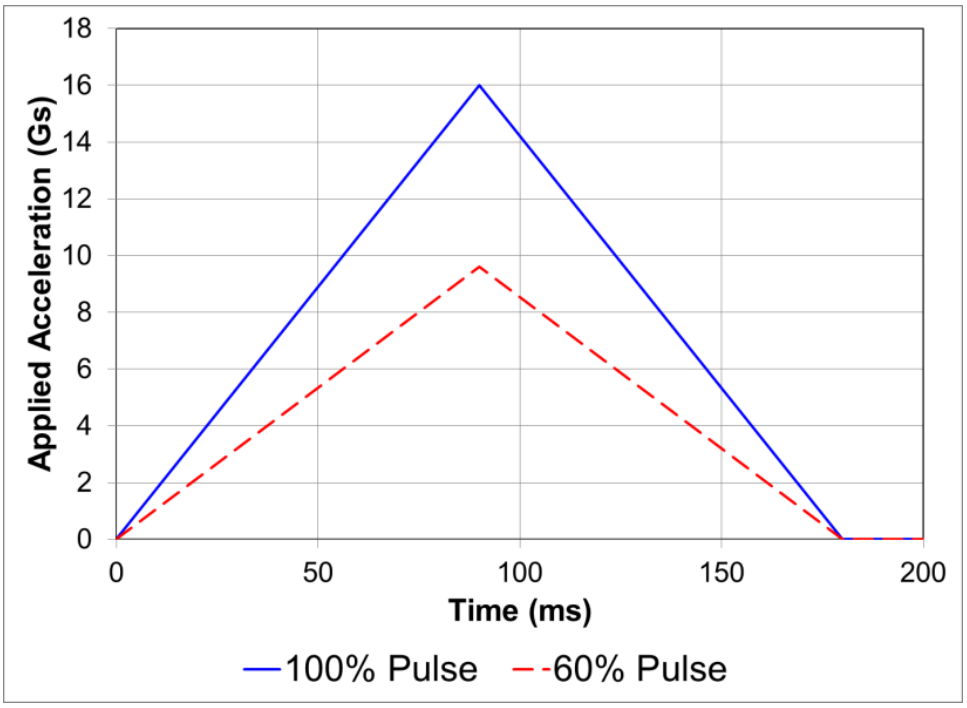

Figure 12: Applied Acceleration Fields

A range of seat installation angles were simulated by adjusting the X- and Y-components of the acceleration field ranging from 0° to 60° with respect to the seat centerline (Table 1). All simulations included a Z-component equal to a constant value of -1.0g.

Table 1: Pulse Peak G by Directional Component

Seat Orientation	0°	30°	45°	60°
X-component	16.0g	13.9g	11.3g	8.0g
Y-component	0.0g	8.0g	11.3g	13.9g
Z-component	-1.0g	-1.0g	-1.0g	-1.0g

Test-Model Deviations

The models were set up to be identical to allow for evaluation of trends. The physical tests were originally run for other purposes (specifically to support the postmortem human subjects project) and run across 4 years. There are numerous variations within the test series and therefore differences between the model initial/boundary conditions and the test conditions.

ATD Initial Position: The initial position of the v-ATD in the seat is identical for all simulations. In the physical tests, the ATD is reseated before each test. While the procedure used by CAMI to seat an ATD is fairly repeatable, variations still occur. For the 2016 tests, the H-pt X-position varied ± 0.2 inches (with an additional test at 0.8 inches off the average) and the Z-position varied ± 0.3 inches. Head CG X-position varied ± 0.65 inches and the Z-position varied ± 0.35 inches. Also, wear of the seat cushion and ATD pelvis can change the natural 1-G position of the ATD. As stated above, the referenced tests crossed 4 years and ATD pelvis degradation was observed, but not explicitly quantified. Using a single v-ATD initial position is useful for trend analysis because it eliminates a source of variability. For the test-simulation comparisons, the initial position deviations will decrease the level of correlation.

Belt Configuration: Tests conducted in 2012 with the armrest included only a single lap belt, while the 2012 no armrest configurations and all the 2016 tests included both the lap belt and the body centered belt. For consistency, all simulations included both the standard lap belt and the body centered belt. The body-centered belt reduces the lateral motion of the pelvis and therefore reduces the impact force on the armrest. Therefore, the model will likely under-predict the armrest force in the 2012 tests.

Belt to Cushion Interaction: Due to the width of the seat, tightening the lap belt resulted in compression of the seat bottom cushion (Figure 13). This interaction was not included in the model. It is unknown how much this interaction affects the motion of the ATD.

Figure 13: Compression of Seat Bottom Cushion by Lap Belt (Red Circle)

Cardboard: The armrest was lined with very low strength honeycomb cardboard (the specific strength is unknown). For the physical tests, this cardboard acts as a mild dampener and provides a witness mark (Figure 14). Due to the low crush strength, the cardboard was not included in the model. This is not expected to affect the comparison, but is noted for completeness.

Figure 14: Cardboard Condition Pre-test (L), Post-test (R)

Leg Restraints: For the physical tests, the lower legs were restrained with belt webbing (Figure 15). This was done to eliminate potential issues when these test configurations were repeated with post mortem human subjects. The setup also replicated a pod arrangement where the legs are trapped by the structure. Based on feedback from seat manufacturers, this arrangement is not expected to be predominant in the fleet. Therefore the simulations were run with the legs free to flail. Tests of forward-facing seats have shown that restricting the leg motion can reduce the head path in lap belt only occupants, presumably because it changes the amount of pelvic

rotation [14]. Due to the presence of a body-centered belt, the leg motion may have a smaller effect on the occupant kinematics; however, it is likely to cause some deviation in the comparison between test and simulation. For tests with a shoulder harness, the difference in leg motion is likely to have a limited effect on the torso motion.

Figure 15: Leg Restraints

SIMULATION MATRIX AND RESULTS

Thirty-two simulations were run in Madymo Version 7.6 on a multi-core desktop computer using four cores. Simulations were run for 250 ms with a time step of $1.0E^{-6}$ ms. The frequency of output for simulation results was selected to match the physical data: 10 kHz for electronic instrumentation and 1 kHz for positions and rotations. The signals were filtered according to SAE J211/1 [15]. In multiple simulations, instabilities in the simulations resulted in large values for some outputs, typically after 200ms. When these instabilities occurred after the peak occupant motion, they were excluded from the reported data. Lumbar and T12 forces from Madymo have an initial compression, of 63 lb and 58 lb respectively. The simulation results were post-processed to zero out the initial compressions. This section is split into two categories: model evaluation and configuration evaluation.

Model Evaluation

The simulation results were compared with the test data for eight configurations to check for reasonableness and define a baseline of model correlation. One test-simulation pair was defined for the seat with and without an armrest, with and without a shoulder strap, and at 30° and 45°, as shown in Tables 2 and 3. The run numbers are based on standard CAMI naming convention; simulations are labeled with an 'S,' physical tests are labeled with an 'A,' the year of the run is recorded using two digits, and the next three numbers indicate the chronological order for the run. For example, the first simulation for 2016 is labeled S16001, while the 27th physical test of 2012 is A12027. All force values are in pounds.

45° Installations

At 45°, the occupant is loaded equally in the fore-aft direction and the lateral direction. In the lap belt only configurations, this resulted in significant flail (Figures 16 and 17). In the no armrest case, the torso flail appears to be similar in a qualitative sense, however the bending in the spine may be different due to the leg restraints in the physical test. For the armrest scenarios, the lower portion of the occupant's chest contacts the armrest. The location of contact appears to be similar. The addition of a shoulder harness significantly reduces the torso flail (Figure 18). There is no apparent contact between the occupant and the armrest for the shoulder harness configurations. The impact of the differences in leg restraints appears to be smaller than in the lap belt-only condition.

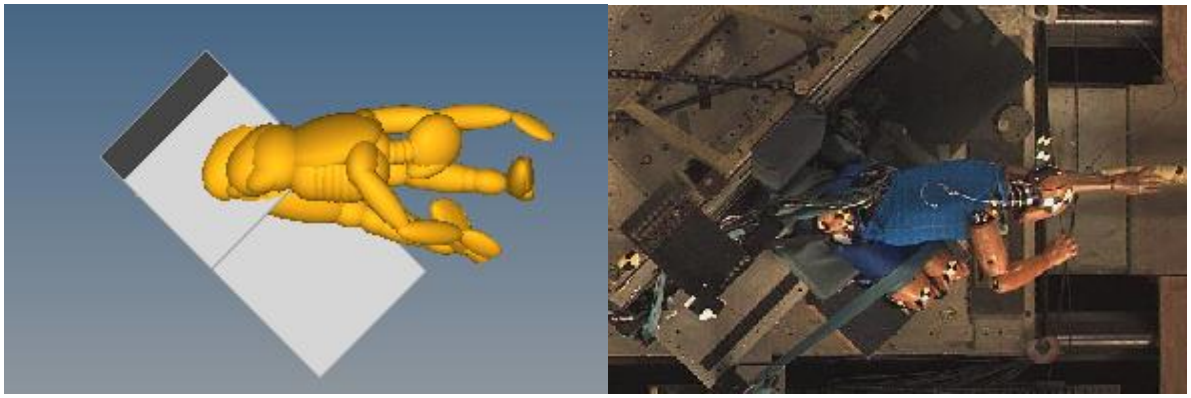

Figure 16: Occupant Flail: No Armrest, Lap Belt Only, 45°

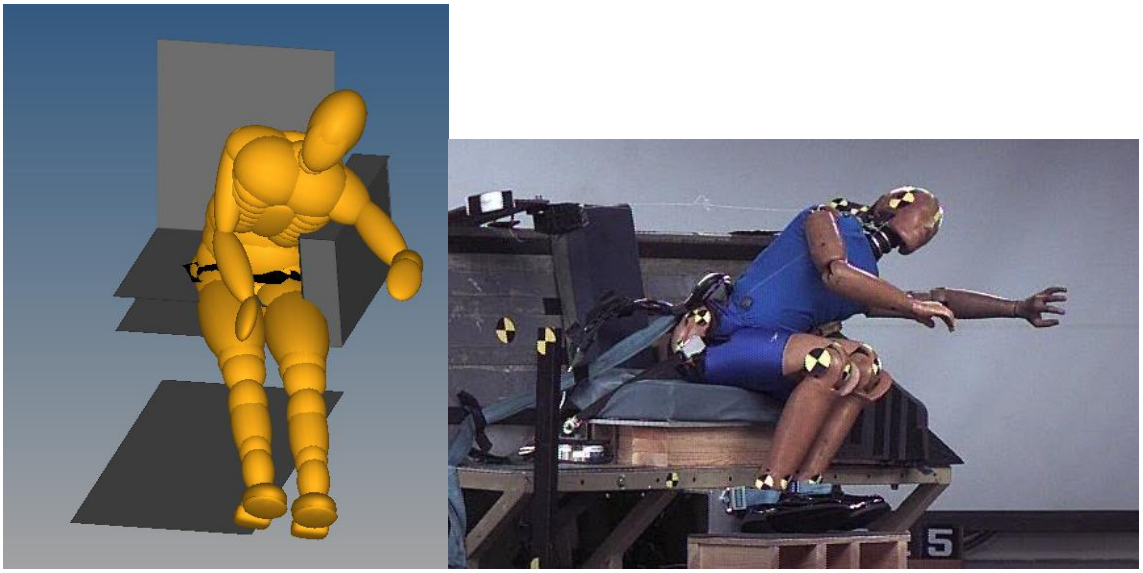

Figure 17: Occupant Flail: Armrest, Lap Belt Only, 45°

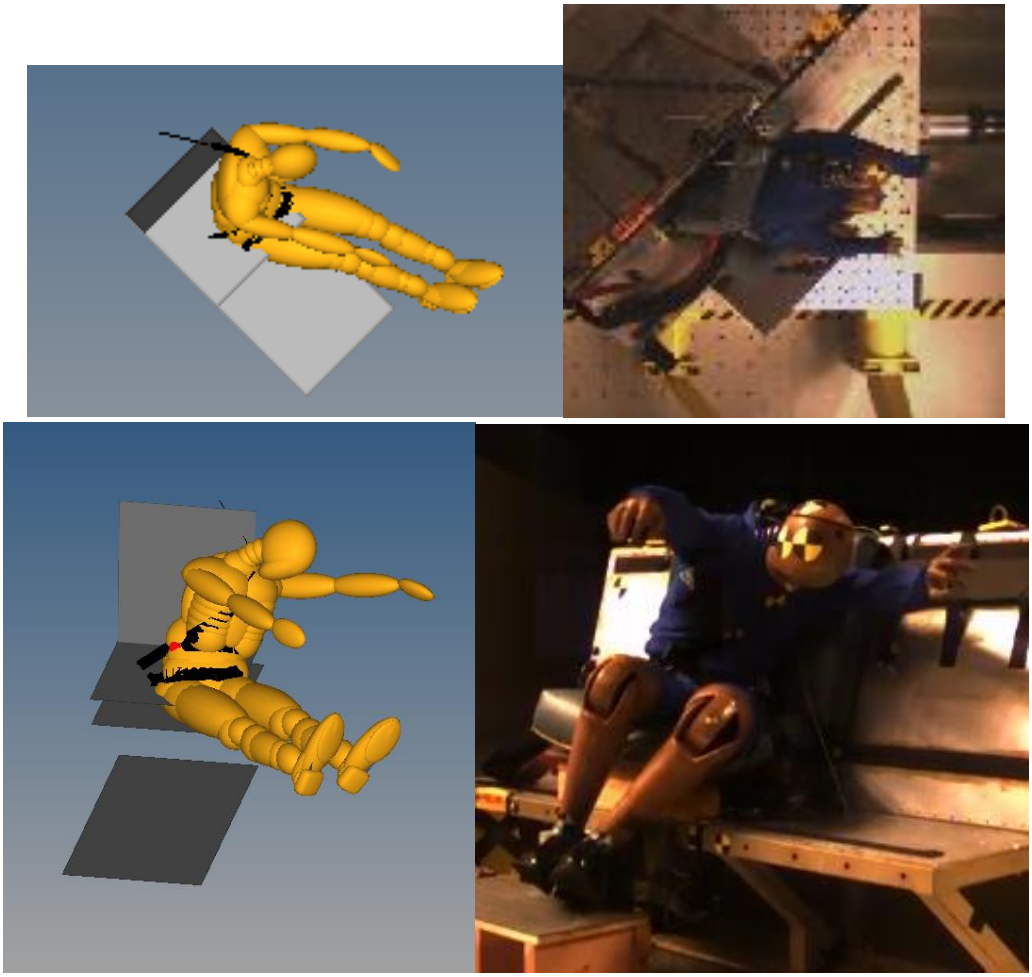

Figure 18: Occupant Flail: No Armrest, Shoulder Harness, 45°

The lap belt only configuration without an armrest has a similar total load (with a 135 lb difference between the sum of the lumbar and T12 loads), but a significantly different distribution (Table 2). The simulation showed nearly twice as much force at T12 than at the lumbar, while the test data showed similar values between the lumbar and T12 (Figure 19). The timing of the loads is also different between the test and simulation, with the simulation showing an earlier onset. In the simulation of the lap belt only armrest configuration, all three loads were lower than the physical test data. When using a shoulder harness, with and without the armrest, the simulated spinal loads were roughly one third of the test results, and the armrest force was more than 3 times higher in the simulation. The peak shoulder belt loads were within 200 lb (14%).

Table 2: Test-Simulation Peak Comparison for 45° Configuration

	S16005	A12024	S16013	A12025	S16021	A16036	S16029	A16035
Peak G's	16	16.7	16	16.8	16	16.3	16	16.6
Configuration	No rest	No rest	Armrest	Armrest	No rest	No rest	Armrest	Armrest
Restraint	Lap belt	Lap belt	Lap belt	Lap belt	Shoulder	Shoulder	Shoulder	Shoulder
Orientation	45°	45°	45°	45°	45°	45°	45°	45°
Lumbar Fz	1591	2017	1868	2829	-305	-974	-299	-721
T12 Fz	2995	2434	2021	2841	-331	-950	-286	-740
Armrest Force	N/A	N/A	-1779	-2348	N/A	N/A	-3503	-1046
Strap Load	N/A	N/A	N/A	N/A	1349	1391	1207	1405

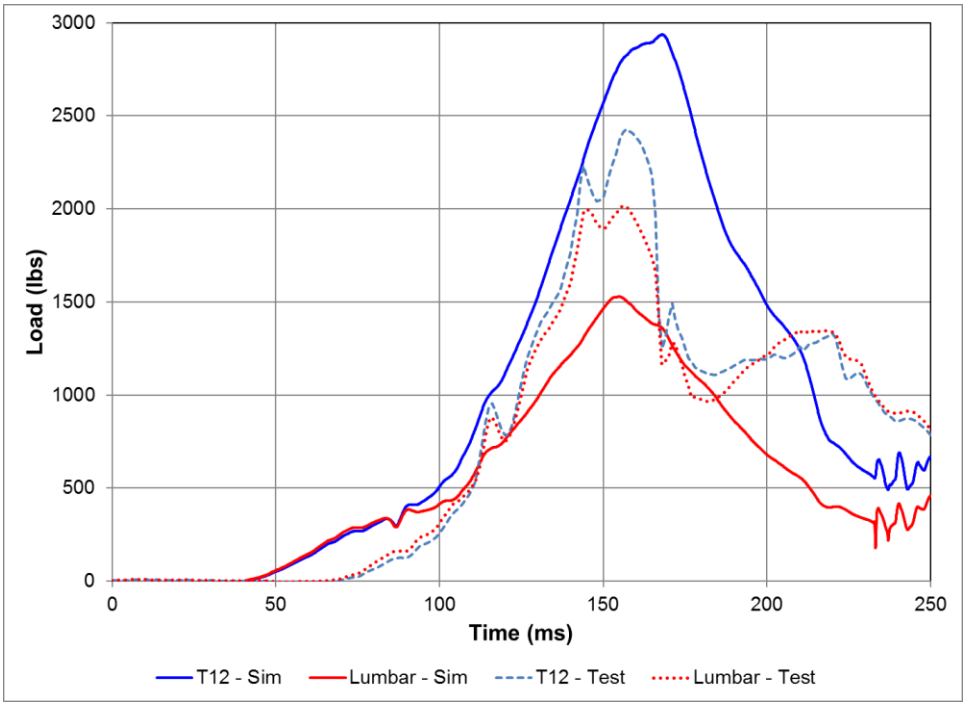

Figure 19: 45°, Lap Belt Only

30° Installations

At 30°, the occupant is loaded more fore-aft than laterally. When comparing the test and simulation loads, similar trends appear as seen in the 45° configurations. For the lap belt-only no armrest configuration, the distribution of spinal forces differs from test to simulation, but the sum of those forces is somewhat similar (difference: 488 lb, approximately10%). The lap belt only armrest case is similar, again showing a different distribution, but similar total load (difference: 351 lb, approximately 7%). The armrest force is within 100 lb (7%). For the shoulder harness cases, the model strongly under-predicts the spinal forces (between one-quarter and one-third as much load as the test values) and over-predicts the armrest force (300% greater), but it does a reasonable job of capturing the shoulder harness force (15% under-prediction). Note that the strap load from test A16037 had to be estimated because of a failure on that channel. For each test in this series, one webbing transducer was placed between the occupant and the belt guide (referred to as the upper shoulder belt tension) and another transducer was placed between the belt guide and the lower anchor point. The upper

strap load in test A16037 was estimated based on the measured lower load and the ratio between upper and lower shoulder belt tension measures in the other tests in this series.

Table 3: Test-Simulation Peak Comparison for 30° Configuration

	S16003	A12027	S16011	A12026	S16019	A16037	S16027	A16039
Peak G's	16	16.4	16	17.1	16	16.5	16	16.1
Configuration	No rest	No rest	Armrest	Armrest	No rest	No rest	Armrest	Armrest
Restraint	Lap belt	Lap belt	Lap belt	Lap belt	Shoulder	Shoulder	Shoulder	Shoulder
Orientation	30°	30°	30°	30°	30°	30°	30°	30°
Lumbar Fz	1932	2135	1864	2374	-317	-972	-332	-1245
T12 Fz	3327	2636	2752	2593	-348	-938	-314	-1191
Armrest Force	N/A	N/A	-1319	-1229	N/A	N/A	-1350	-457
Strap Load	N/A	N/A	N/A	N/A	1273	1410*	1154	1359

*Sensor failure, value estimated based on measured lower shoulder belt tension and ratio between upper and lower shoulder belt tension measures in the other tests in this series.

Remarks

Overall, the model results are significantly different from the test results. The model under-predicts spinal loads with a shoulder strap and has a different distribution of spinal loads in the lap belt-only configurations. Some discrepancies are likely due to different initial and boundary conditions; however, the different distribution of loads between the lumbar and T12 locations suggests that the interaction of the lap belt on the pelvis is inaccurate or the lumbar joint model needs refinement. A lap belt interaction issue was observed in forward facing simulations with the Madymo Hybrid II v-ATD [16] and led to a modification of that pelvis [10]. The modification involved creating a more geometrically accurate surface for the pelvis using facets instead of ellipsoids. A similar modification would likely benefit the FAA Hybrid III v-ATD. Due to the observed deviations, any conclusions drawn from the results of the trend analysis should be considered preliminary.

Configuration Evaluation

The full set of 32 simulations was used to evaluate trends based on the configurations and to observe the performance of the model as a function of seat installation angle. This set includes a seat installation angle range from 0° and 60°, the armrest and no armrest conditions, with and without a shoulder harness, and two input pulses. The results are tabulated by belt and armrest configuration in Tables 4, 5, 6 and 7. All force values are in pounds.

Lap Belt, No Armrest

For the lap belt-only, no armrest case, the ratio of spinal loads are consistent within the set of impact severity (Table 4). As shown in Figure 20, at both load cells and both pulse levels, the peak loads are linear ($R^2 > 0.92$). The differing slopes of the trend lines, approximately 20 lb/deg for 16g and 7 lb/deg for 9.6g, may be related to the same issue that resulted in the different ratio of spinal loads shown in Figure 19. The overall trend suggests that spinal Fz load decreases with impact angle, which, if reproducible, would assist in defining a critical installation angle for certification testing for the current injury criteria.

Table 4: Peak Values for Lap Belt Only, No Armrest Configuration

	S16001	S16003	S16005	S16007	S16002	S16004	S16006	S16008
Peak G's	16	16	16	16	9.6	9.6	9.6	9.6
Configuration	No rest	No rest	No rest	No rest	No rest	No rest	No rest	No rest
Restraint	Lap belt	Lap belt	Lap belt	Lap belt	Lap belt	Lap belt	Lap belt	Lap belt
Orientation	0°	30°	45°	60°	0°	30°	45°	60°
Lumbar Fz	2564	1932	1591	1461	1193	975	799	751
T12 Fz	3699	3327	2995	2433	1644	1496	1395	1203

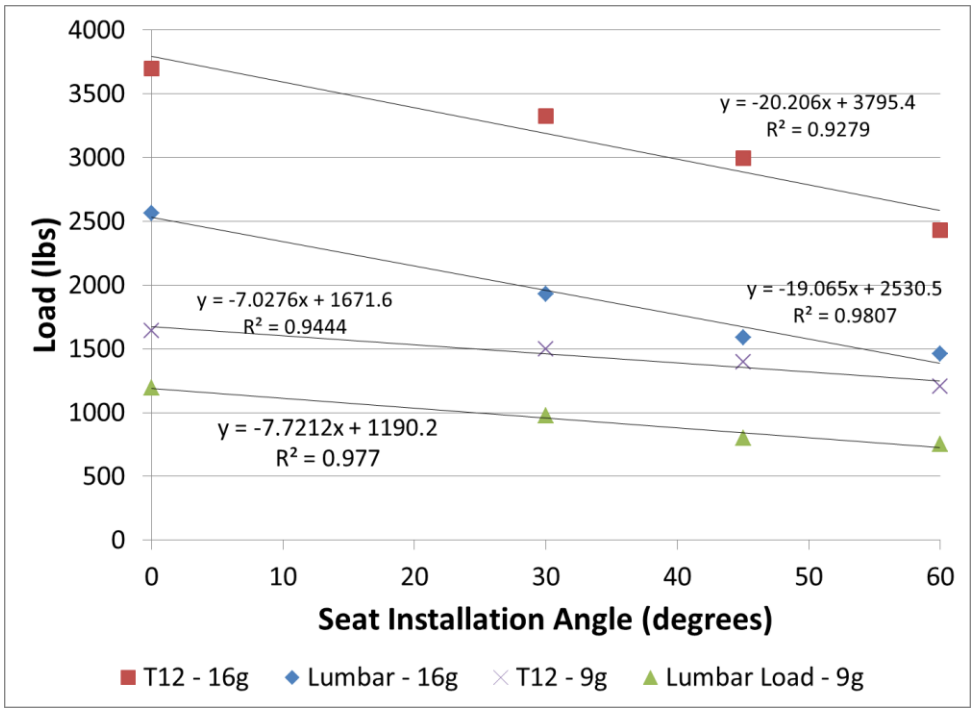

Figure 20: Spinal Loads vs. Angle for Lap Belt Only, No Armrest

Lap Belt With Armrest

For the lap belt-only armrest case, the spinal loads are not linear, likely due to the differences in the amount of momentum that is off-loaded to the armrest (Table 5, Figure 21). A plot of the armrest force highlights the different interactions (Figure 22). At zero degrees there is no contact between the occupant and the armrest, which is expected. As the angle increases, the lateral contact force increases exponentially, although it does so at different rates based on the impact severity. The high armrest load observed in the 16g, 60° case seems to be related to a numerical instability where the hip rapidly moves away from the armrest in less than 10 ms (Figure 23).

Table 5: Peak Values for Lap Belt Only, WithArmrest Configuration at 16g

	S16009	S16011	S16013	S16015	S16010	S16012	S16014	S16016
Peak G's	16	16	16	16	9.6	9.6	9.6	9.6
Configuration	Armrest	Armrest	Armrest	Armrest	Armrest	Armrest	Armrest	Armrest
Restraint	Lap belt	Lap belt	Lap belt	Lap belt	Lap belt	Lap belt	Lap belt	Lap belt
Orientation	0°	30°	45°	60°	0°	30°	45°	60°
Lumbar Fz	2603	1864	1868	2862	1181	865	944	948
T12 Fz	3626	2752	2021	3114	1629	1192	1048	958
Armrest Force	45	1319	1779	4689	52	201	721	1592

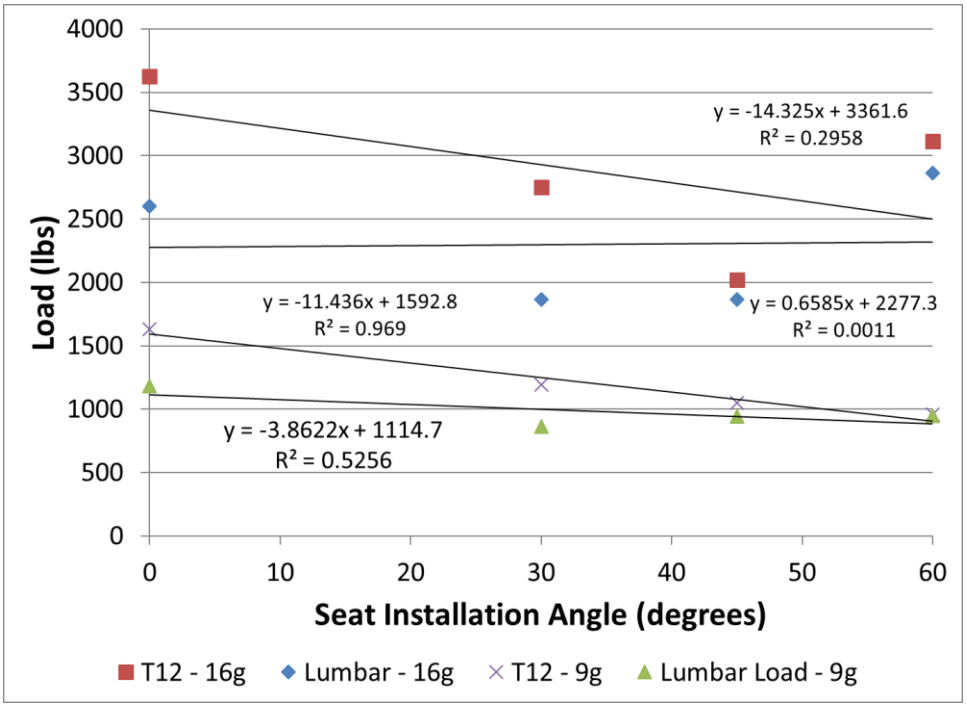

Figure 21: Spinal Loads vs. Angle for Lap Belt Only, With Armrest

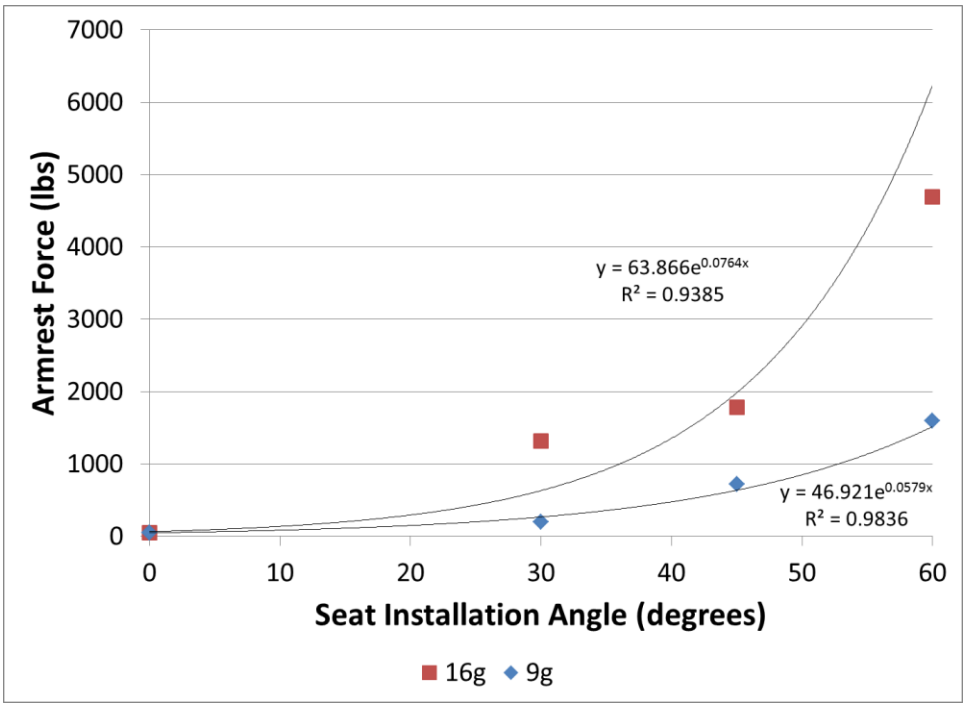

Figure 22: Armrest Force, Lap Belt Only Configuration

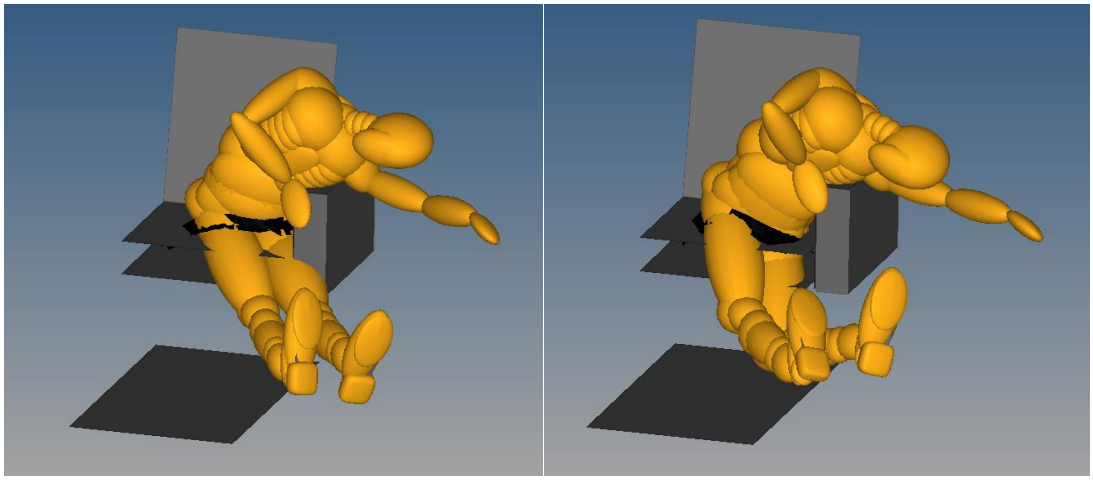

Figure 23: Rapid Hip Motion Away From Armrest, T=149 ms (L), T=158 ms (R)

Shoulder Belt, No Armrest

For the shoulder belt and no armrest case, the lumbar and T12 loads are very similar, as is expected because the occupant has much less flail (Table 6). A linear trend appears for the 30° to 60° scenarios, but the 0° case appears to be an outlier (Figure 24). In both 0° simulations, the shoulder harness slides off the occupant's shoulder (Figure 25). This may be due to the location of the shoulder harness to lap belt attachment point (near the ATD centerline), which was designed for purely side-facing seats and not optimized for a forward-facing seat. Across all orientations, the 9g simulations produced more spinal compression than the 16g simulations, as exemplified in Figure 26. This may seem counterintuitive; however, an

understanding of the opposing loads provides an explanation. The 16g pulse will propel the occupant forward with more severity than the 9.6g pulse. This creates both more spinal tension from flail and more spinal compression from the shoulder strap, relative to the 9.6g pulse. The summation of these loads may not necessarily result in higher lumbar compression in the 16g case.

Table 6: Peak Values for Shoulder Belt, No Armrest Configuration at 16g

	S16017	S16019	S16021	S16023	S16018	S16020	S16022	S16024
Peak G's	16	16	16	16	9.6	9.6	9.6	9.6
Configuration	No rest	No rest	No rest	No rest	No rest	No rest	No rest	No rest
Restraint	Shoulder	Shoulder	Shoulder	Shoulder	Shoulder	Shoulder	Shoulder	Shoulder
Orientation	0°	30°	45°	60°	0°	30°	45°	60°
Lumbar Fz	-273	-317	-305	-282	-379	-400	-366	-337
T12 Fz	-265	-348	-331	-285	-381	-414	-379	-341
Strap Load	1315	1273	1349	1467	836	726	774	880

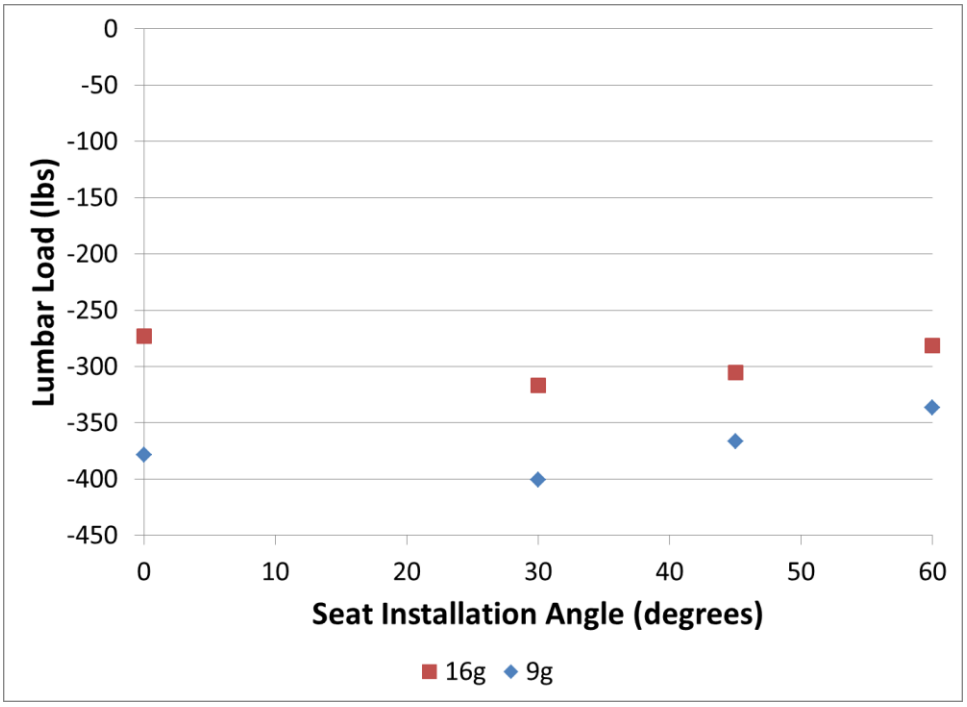

Figure 24: Lumbar Load for Shoulder Belt, No Armrest Configuration

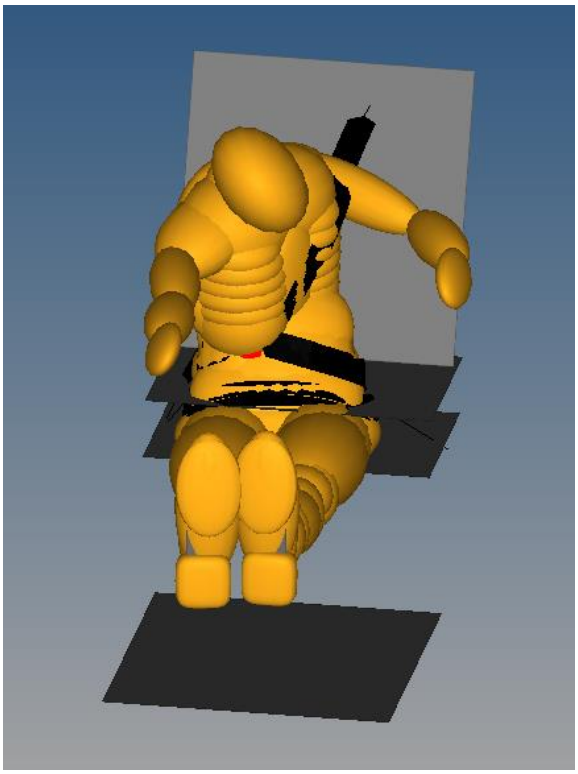

Figure 25: Shoulder Belt Sliding Off Occupant for 0° Orientation

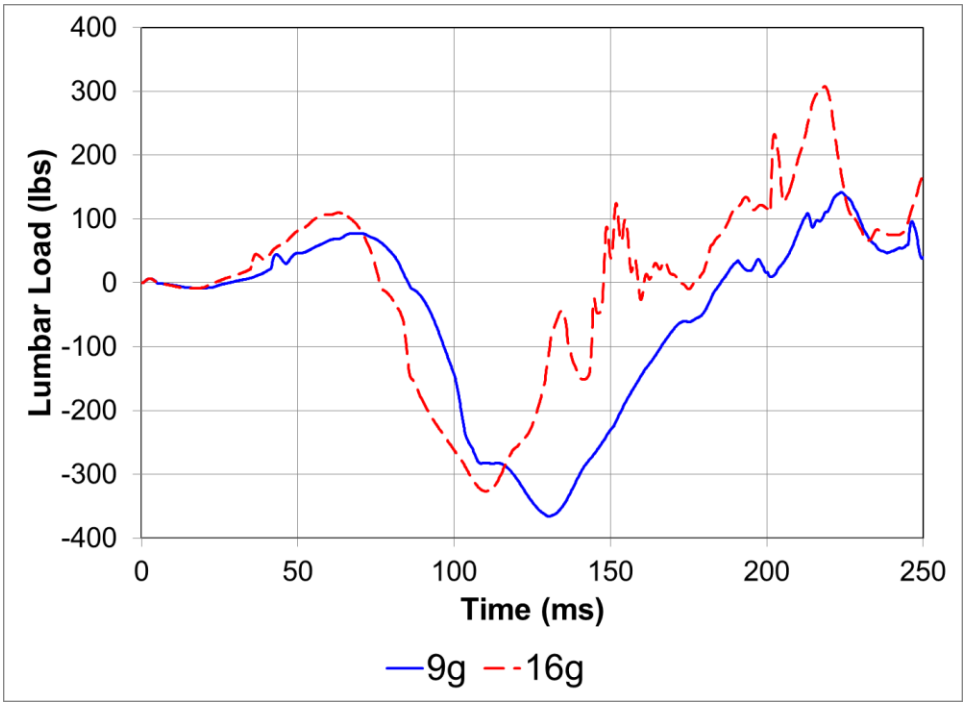

Figure 26: Lumbar Load for 45° Shoulder Belt, Armrest Case

Shoulder Belt With Armrest

For the shoulder harness with an armrest case, there was little difference between the lumbar and T12 loads, and the loads did not vary much across the orientations (Table 7). As with the

no armrest simulations, the occupant slides out of the shoulder harness during the zero-degree simulations.

Table 7: Peak Values for Shoulder Belt and Armrest Configuration at 16g

	S16025	S16027	S16029	S16031	S16026	S16028	S16030	S16032
Peak G's	16	16	16	16	9.6	9.6	9.6	9.6
Configuration	Armrest	Armrest	Armrest	Armrest	Armrest	Armrest	Armrest	Armrest
Restraint	Shoulder	Shoulder	Shoulder	Shoulder	Shoulder	Shoulder	Shoulder	Shoulder
Orientation	0°	30°	45°	60°	0°	30°	45°	60°
Lumbar Fz	-273	-332	-299	-346	-379	-390	-337	-330
T12 Fz	-265	-314	-286	-352	-382	-424	-341	-319
Strap Load	1315	1154	1207	1161	836	665	691	648
Armrest Force	0	1350	3503	5292	0	793	1063	2597

OBSERVATIONS

Model Evaluation

The automotive Hybrid III was developed for pure forward-loading conditions. The modifications of the ATD to create the FAA version focused on performance in the forward and vertical loading directions. The developer of the Madymo FAA Hybrid III evaluated the model against these types of tests and component tests designed with these loading conditions in mind. There has been limited usage from the aviation seating industry for the FAA Hybrid III v-ATD, particularly in the Madymo platform. As such, the model developer has not validated, nor calibrated, the model for the configurations simulated in this project. Because of this, it is understandable that the model is not as accurate in oblique configurations as it is in pure fore-aft configurations. For the model to be accurate enough for certification, changes to the model are needed.

Trend Analysis

The model appears to be robust across the range of configurations simulated for this project. In the lap belt only without an armrest configuration, the spinal loads were linear across angles, but had different slopes further suggesting that improvements are needed to the model. When a shoulder belt is included, the spinal loads became compressive and were generally low. The model with the shoulder belt produced mostly linear results across impact angles, showing the expected trends. The Madymo FAA Hybrid III v-ATD appears to require further evaluation and possible changes prior to use to predict occupant injury in oblique loading configurations.

REFERENCES

[1] Code of Federal Regulations, Title 14, Part 25.562. Emergency Landing Dynamic Conditions. Washington, DC: U.S. Government Printing Office, 1988.

[2] Department of Transportation. 2000. Federal Aviation Administration, Information: Use of the Hybrid III Anthropomorphic Test Dummy in Seat Dynamic Testing. Washington, DC. Federal Aviation Administration, Memorandum, AIR-100-3-3-2000, March.

[3] Federal Aviation Administration Policy ANM-25-03-R1 - Technical Criteria for Approving Side-Facing Seats. Washington, DC: Federal Aviation Administration, 2012.

[4] Federal Aviation Administration Policy PS-AIR-25-27 - Technical Criteria for Approving Oblique Seats. Washington, DC: Federal Aviation Administration, 2018.

[5] Taylor A, DeWeese R, Moorcroft D. "Initial Evaluation of ATDs for Testing of Obliquely Oriented Seats," The Seventh Triennial International Fire & Cabin Safety Research Conference, Dec 2-5, 2013.

[6] Humm J, Peterson B, Pintar F, Yoganandan N, Moorcroft D, Taylor A, DeWeese R. "Injuries to Post Mortem Human Surrogates in Oblique Aircraft Seat Environment," Biomedical Sciences Instrumentation, April 2015; 51:431-438.

[7] Humm J, Moorcroft D, Yoganandan N, DeWeese R, Taylor A, Pintar F. "Preliminary FAA-Hybrid III Spinal Injury Criteria for Oblique Aviation Seats," ASME International Mechanical Engineering Congress & Exposition paper and presentation (Nov 2015).

[8] Humm J, Yoganandan N, Pintar F, DeWeese R, Moorcroft D, Taylor A, Peterson B. Responses and Injuries to PMHS in Side-Facing and Oblique Seats in Horizontal Longitudinal Sled Tests per FAA Emergency Landing Conditions. Stapp Car Crash Journal, Vol. 60 (November 2016), pp. 135-163.

[9] SAE International. Performance Standards for Side-Facing Seats in Civil Rotorcraft, Transport Aircraft, and General Aviation Aircraft. Warrendale, PA: SAE International. SAE Aerospace Standard 8049C, 2015.

[10] TASS International. "Madymo Model manual version 7.6," TASS International, Helmond, The Netherlands. 2015.

[11] Code of Federal Regulations, Title 49, Part 572, Subparts B and E. Anthropomorphic Test Devices. Washington, DC: U.S. Government Printing Office, 2006.

[12] SAE International. Analytical Methods for Aircraft Seat Design and Evaluation. Warrendale, PA: SAE International. SAE Aerospace Recommended Practice 5765A, 2015.

[13] Moorcroft D. "Performance of a Numerical Model of the ES-2re as a Function of Impact Angle," The Seventh Triennial International Fire & Cabin Safety Research Conference, Dec 2-5, 2013.

[14] DeWeese R, Moorcroft D. “Kinematics of Lap Belt Restrained Occupants,” Aerospace Structural Impact Dynamics International Conference, Nov 6-7, 2012.

[15] SAE International. Instrumentation for Impact Test – Part 1- Electronic Instrumentation. Warrendale, PA: SAE International. Surface Vehicle Recommended Practice No: J211-1, 2014.

[16] Moorcroft D. “Evaluation of the Madymo Hybrid II Dummy Model in an Aviation-Specific Crash Scenario,” SAE General Aviation Technology Conference, Aug 30, 2006.